ISSN 0389-4010
UDC 621.438
532.5

TECHNICAL REPORT OF NATIONAL AEROSPACE LABORATORY

TR-1021T

DECAY OF SECONDARY FLOW AND THE ASSOCIATED LOSS VARIATION DOWNSTREAM OF AN ANNULAR TURBINE STATOR CASCADE

Atsumasa YAMAMOTO • Hiroyuki NOUSE

April 1989

NATIONAL AEROSPACE LABORATORY

CHŌFU, TOKYO, JAPAN

Decay of Secondary Flow and the Associated Loss Variation Downstream of an Annular Turbine Stator Cascade*

A. Yamamoto**
and
H. Nouse**

ABSTRACT

Using a five-hole pitot tube and a total pressure probe, the flows downstream of an annular turbine stator cascade were surveyed in detail at seven serial measuring planes, and decay of the secondary flow and variation of the associated total pressure loss were analyzed. Effects of rotation of the hub endwall downstream of the cascade and effects of secondary air injection from the hub endwall on the secondary flow and on the loss were also analyzed.

概　　要

本報告は，環状タービン静翼列下流7断面において5孔ピトー管と全圧管により流れを詳細に測定し，翼列で発生した二次流れとそれに伴なう損失の下流での減衰の模様について述べたものである。また，二次流れと損失に及ぼす翼根部側エンドウォールの回転の影響およびそのエンドウォールからの吹出し流の影響についても議論した。

NOMENCLATURE

Patm	=	Atmospheric pressure
Ps	=	Static pressure
Pt	=	Total pressure
Uh	=	Peripheral velocity of rotating hub surface
Vm	=	Measured flow velocity
Vp	=	Radial flow velocity
$\vec{Vs}$	=	Secondary flow vector
Vs, yz	=	Secondary flow velocity component normal to Vp
Vy	=	Circumferential flow velocity
Vz	=	Axial flow velocity
W	=	Projected velocity of Vm onto cylindrical surface
$\theta p, \theta_y$	=	Pitch angle and yaw angle of flow
θ_y, set	=	Setting angle of five-hole pitot tube
β	=	Ratio of injection air to main flow (mass flow ratio)
ΔPt	=	Total pressure difference defined by

* Received 15, February 1989
** Aeroengine Division

Eq. (8)

$\Delta\vec{V}s$ = Difference of secondary flow vector defined by Eq. (5)

$-$ = Average

Introduction

For development of high-efficiency gas turbines, such as current air-cooled turbines adopted in the high-temperature turbine stage, the internal flow mechanisms have been studied with various types of cascades to reduce the losses and improve the design methods. For annular turbine cascades, however, only a few papers on the complex internal flows have been presented so far; Sjolander[1] Sieverding et al.[2], Hunter[3], and recently Moustapha[4] and Yamamoto and Yanagi[5] Knowledge of effects of the cooling-air on the internal flows is also important in cooled-turbines but has been very limited.

In a serial study at NAL to investigate secondary flows and the associated losses in turbines, a low-speed annular turbine test facility with a fully automatic measuring system has been widely used. The system was designed to be able to detect even weak effects of cooling (secondary) air[6]. The study so far includes flow measurements with a five-hole pitot tube and a total pressure probe, at nine measuring planes before, within and after the stator cascade. The study includes also the cases with/without the downstream rotor, and with/without secondary (cooling) air injection from the stator blade surfaces and from the hub endwall downstream of the stator. Some of the results with the secondary air injection have already been presented by the author et al.[6].

The major purpose of the present paper is to discuss the cascade swirling wake flow and its decay experimentally, because knowledge of such swirling wake flow and its decay is important for designing efficient downstream blade rows and for reducing the noise caused by the interaction between upstream and downstream blades, and because due to the lack of reliable experimental data on turbulent swirling flows, even this relatively simple class of swirling flow has not been accurately predicted yet[7]. Effects of the downstream hub endwall rotation and effects of secondary air injection from the hub endwall on the decay are also discussed.

Experimental Facilities

Low Speed Annular Turbine Wind Tunnel

The test rig (Fig. 1) is a suction type wind tunnel with low turbulent inlet flow. The test section has a length of 860 mm. The upper half casing of the test section has a 300 mm, half cylindrical, transparent plexiglass window to allow inspection of the stator and rotor blade rows. Rotation of the rotor is controled by an electric brake motor at a constant speed with less than ± 0.1% fluctuation between 80 and 2000 rpm. The stator row is driven by a pulse motor through a harmonic (plenetary) reduction gear with a resolution of less than 1/200 degree; This is for ease in making the circumferential traverse measurements. The stator has a blade tip clearance of about 0.5 mm, but the clearance is not sealed specifically, so the measured data in the present tests include effects of tip leakage flow.

Test Stator Rows

The present tests were done without the rotor blades. The test stator blades are untwisted having a constant profile from the hub to the tip. The blades were made of aluminum by the wire-cutting manufacturing method and were bolted on an annular hub endwall in such a way that the lines of the blade trailing edges are normal to the wind tunnel center axis.

The blade profile, cut by the cylindrical surface at the mean radius, is the same as the 'Mean' radius profile of a high temperature turbine for

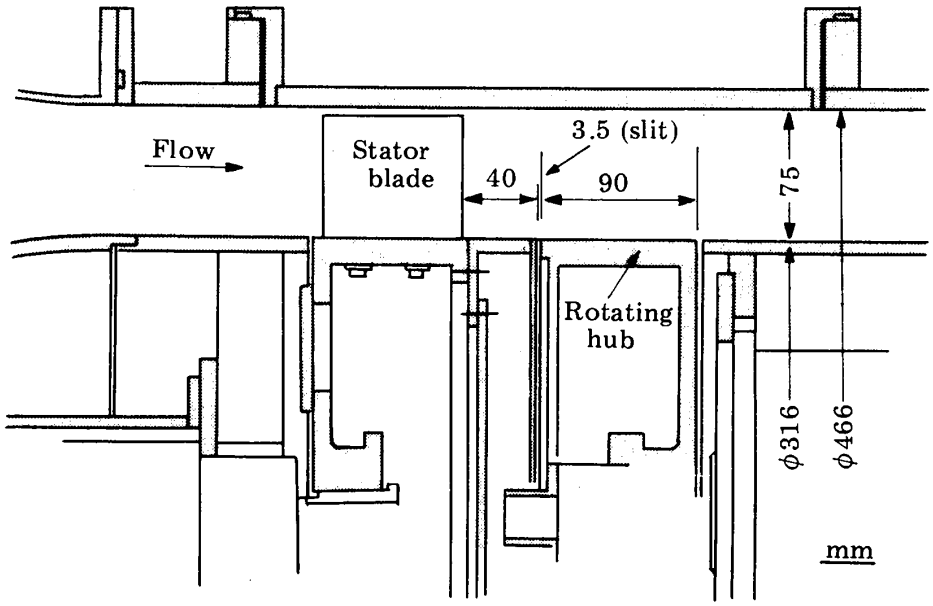

Fig. 1 Test section of NAL low speed turbine

Table 1 Major stator specifications

Hub diameter, d_h	0.316 m
Hub-to-tip ratio, d_h/d_t	0.68
Blade chord (manufactured), c	0.104 m
Aspect ratio, h/c	0.72
Solidity at mean, c/s	1.36
Stagger angle, ξ	39°
Design inlet flow angle, α_1	0°
Design outlet flow angle, α_2	66°

aeroengine use[8]. The blade thickness distribution along the blade camber line is the same as that of Whitney et al.[9]. The major specifications are shown in Table 1.

Test by Fully Automatic Data Acquisition System

The sensors used in the present tests are a cobra type five-hole pitot tube and a shielded type total pressure probe. The latter was designed to accurately sense the total pressure of flow within ± 50 degree inlet angle. The head size of both sensors is 3 mm.

The traverse measurements were made with programmable NC controllers connected to a micro computer; The two sensors located at the inlet and outlet measuring planes were driven by pulse motors in the radial direction; the circumferential positions of the sensors against the stator cascade were set by rotating the cascade itself. The mechanical resolution of the devices are 0.045 mm for the radial traverse and 1/200 degrees for the circumferential traverse; the accuracy of positioning the sensors is thought to be about the same as the mechanical resolution. At each measuring position, the pressures from the pitot tubes and other reference pressures were measured by individual pressure transduces to save the scanning time. A typical traverse time for one test case with 697 measurement points (about 7000 bits of pressure data/test) was about 0.6 hour.

The seven measuring planes analyzed in the paper are shown in Fig. 2; the axial distances of planes 1 and planes 4 to 9 are 19 mm upstream of the blade leading edge, and 3, 33, 80, 115, 145 and 180 mm downstream of the blade trailing edge (each corresponds to about 0.07, 0.78, 1.89, 2.72, 3.43, and 4.26 times the blade chord in the outlet camber line direction). The radial measuring positions nearest to the hub and the tip endwalls are 1.9 mm and 1.95 mm respectively for plane 4, and

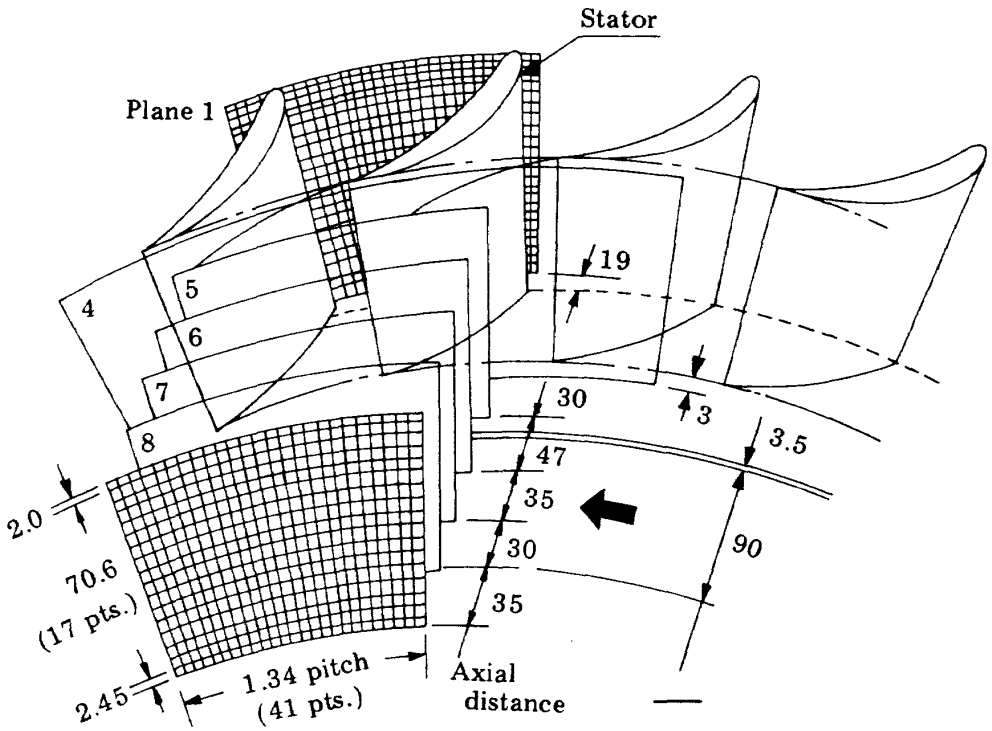

Fig. 2 Traverse measuring planes

2.45 mm and 2.0 mm respectively for other planes; the circumferential traverse width is 3.0 blade pitches for plane 4 and 1.34 for the others. During the traverse measurements, direction of each sensor was always fixed and local flow angles at each measuring point were determined later from three-dimensional calibration carpets of the five-hole pitot tube which was programmed on a VAX 11/750 computer in advance.

The air injected into the main stream from the hub slit was supplied from a rotary compressor. The flow rates were measured by a float-type multi-tube flowmeter with reading accuracy of ± 1%. A programable video tape recorder was used to record the float position during the tests.

Test Conditions

In all tests described in the paper, the inlet flow velocity was kept constant at 13.9 m/s using a Prandtl-type total/static pressure probe located at the midspan of plane 1. The cascade flow Reynolds number based on the blade chord and the cascade outlet flow velocity is about 2.4×10^5.

The test rotational speeds of the rotor hub endwall were 0, 900, 1521 and 1800 rpm in the same direction as that of turbine rotor. Each rotational speed corresponds to Uh/Vz of 0, 1.07, 1.82 and 2.15, respectively.

The test mass flow rate of the injection air was 0%, 0.37% and 0.59%. The air has the same temperature as the main flow (ie., room temperature).

Analysis Method

Definition of Secondary Flow

Fig. 3 shows a method of analyzing the secondary flow vector. W is the velocity component projected onto the cylindrical surface of Vm measured. $\overline{W}$ shows the mass-averaged mean direction of W and the secondary flow is defined as the flow projected onto the plane normal to $\overline{W}$, ie., onto the plane consisting of the a-a direction and the radial p-direction as shown in Fig. 3. The secondary vector $\vec{Vs}$ can be obtained from the

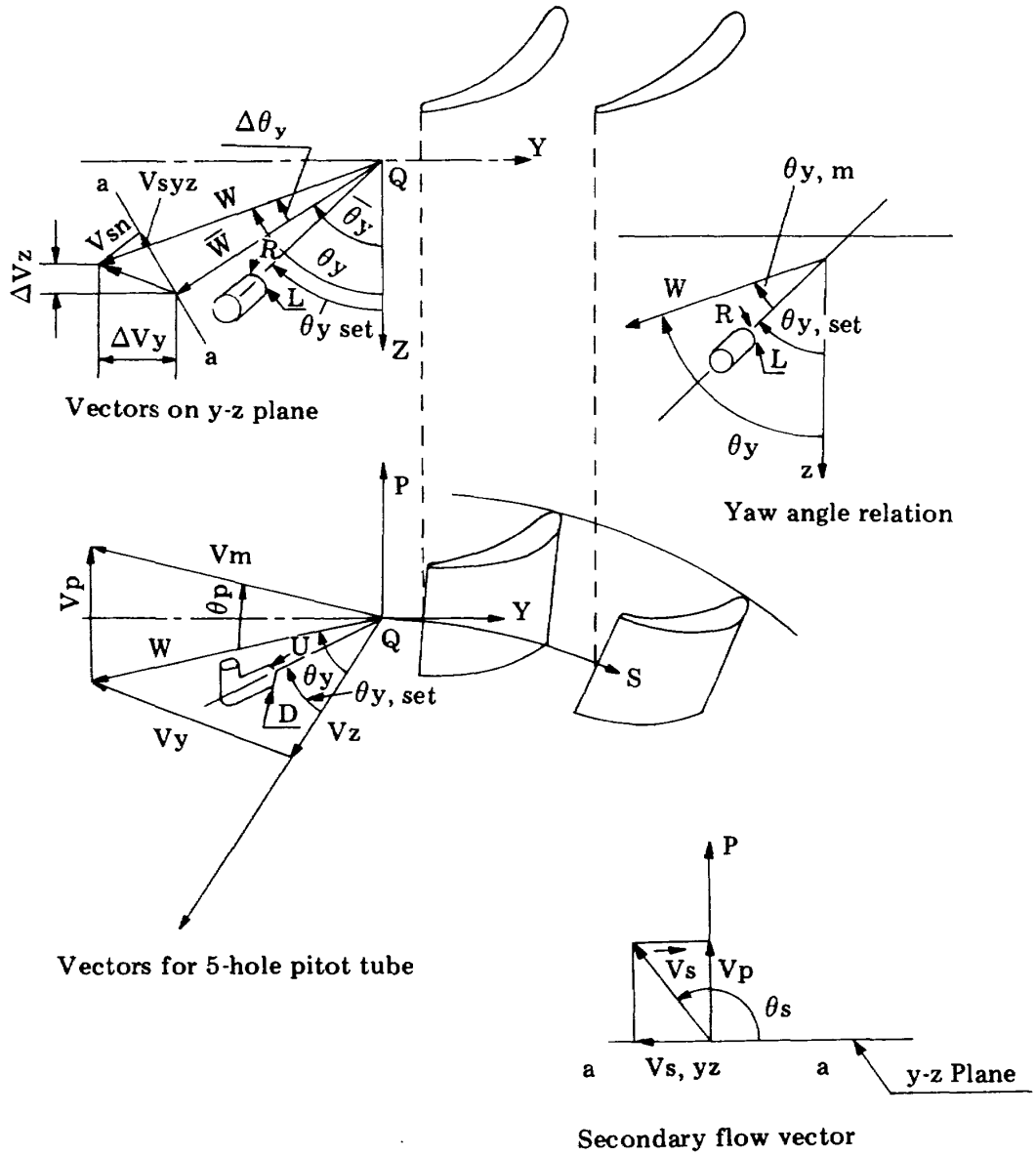

Fig. 3 Secondary flow analysis

spanwise velocity component Vp and the component Vs, yz which is normal to Vp. The two components can be written as follows;

$$Vp = Vm \times \sin\theta p \quad (1)$$

$$Vs, yz = Vm \times \cos\theta p \times \sin\Delta\theta_y \quad (2)$$

where $\Delta\theta_y = \theta_y - \overline{\theta}_y$ (difference between local yaw angle and the mean value $\overline{\theta}_y$). Then $\vec{Vs}$ (Vs, θs) in the polar coordinates is

$$Vs = |\vec{Vs}| = \sqrt{Vp^2 + Vs, yz^2} \quad (3)$$

$$\theta s = \cos^{-1}(Vs, yz / Vs) \times \text{sign}(Vp) \quad (4)$$

The present method has an advantage that, even if there were misalignment of the initial setting yaw angle of the five-hole pitot tube relative to the cascade, there is little effect on the analyzed secondary vector since only the difference of θ_y is included in the analysis.

Method to analyze Weak Effects on Secondary Flow Vectors and on Scaler Quantities

In order to analyze very weak effects of the hub rotation or of the hub injection clearly, two secondary flow vectors at two different rotational conditions (or two different injection con-

ditions) were subtracted each other. The subtractions were made for all corresponding measuring points as follows:

for the secondary flow vectors,

$$\Delta\vec{Vs} = \vec{Vs}, 2 - \vec{Vs}, 1 \quad (5)$$

or

$$\Delta Vs = |\vec{Vs}, 2 - \vec{Vs}, 1| \quad (6)$$

$$\Delta\theta s = \cos -1\,(\Delta Vs, yz / \Delta Vs) \times \text{sign}\,(\Delta Vp) \quad (7)$$

Similarly, for scalar quantities,

$$\Delta Pt = Pt, 2 - Pt, 1 \quad (8)$$

where the suffixies 2 and 1 denote cases with and without the rotation or the injection, respectively. To use this method, it was necessary to position the sensor consistently and keep the flow condition accurately constant through the tests 1 and 2. This technique has already been used successfully to show the effects of coolant injection from blade surfaces on secondary flow fields within the stator cascade[6].

Experimental Results and Discussions

Decay of the Wake Without Hub Rotation and Injection

The contour values of total and static pressures (ie., Pt and Ps) in the following figures are shown as the differences from the atmospheric pressure.

(a) Upstream Flow Field (Plane 1)

Fig. 4 shows the secondary flows at the inlet plane 1 just before the blade row. All vectors shown in the paper were drawn by looking at them from the cascade downstream side. The mark (+) indicates the traverse point from which a secondary vector is drawn.

The secondary flows direct, in general, normal to the constant static pressure lines following the pressure gradient and are going away from the

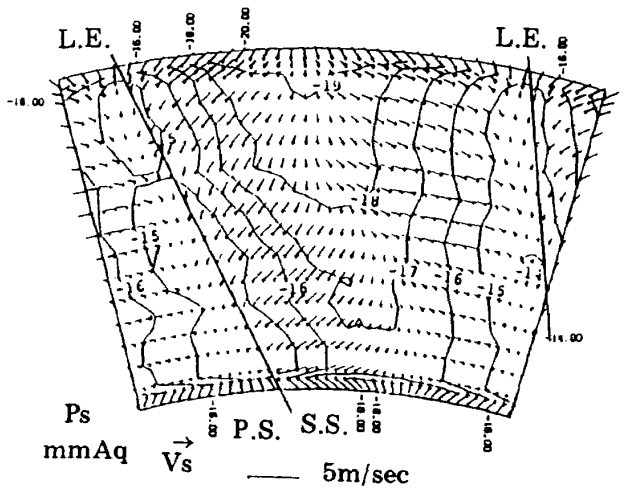

Fig. 4 Upstream flow field (Plane 1)

suction side of the blade leading edge toward the minimum static pressure region near the tip endwall where the flow velocity is highest. The total pressure at the plane, however, was almost uniform (a little higher at the outer region than the inner).

(b) Downstream Flow Fields

At Plane 4. Since the plane is very close to the blade trailing edge and strong shear flows exist, only total pressure surveys were conducted in three blade pitch width using a shielded total pressure probe. The total measuring points are 1900 (19 radial x 100 pichwise) with finer traverse mesh sizes near the trailing edges. Fig. 5 shows that the pressure side edges of the wakes are almost straight corresponding to the straight blade trailing-edge lines. Boundary layers on the blade pressure surfaces are very thin. The low pressure fluids are accumulated on the blade suction surfaces and do not spread widely yet, ie., large loss-free regions still exist between the wakes.

At Plane 5. Fig. 6(a) shows secondary flow vectors superimposed on total pressure contours at plane 5 (about 0.86 chord downstream from the trailing edge along the mean flow direction). The flows contain an inner vortex and an outer vortex, both of which rotate counterclockwise, and also

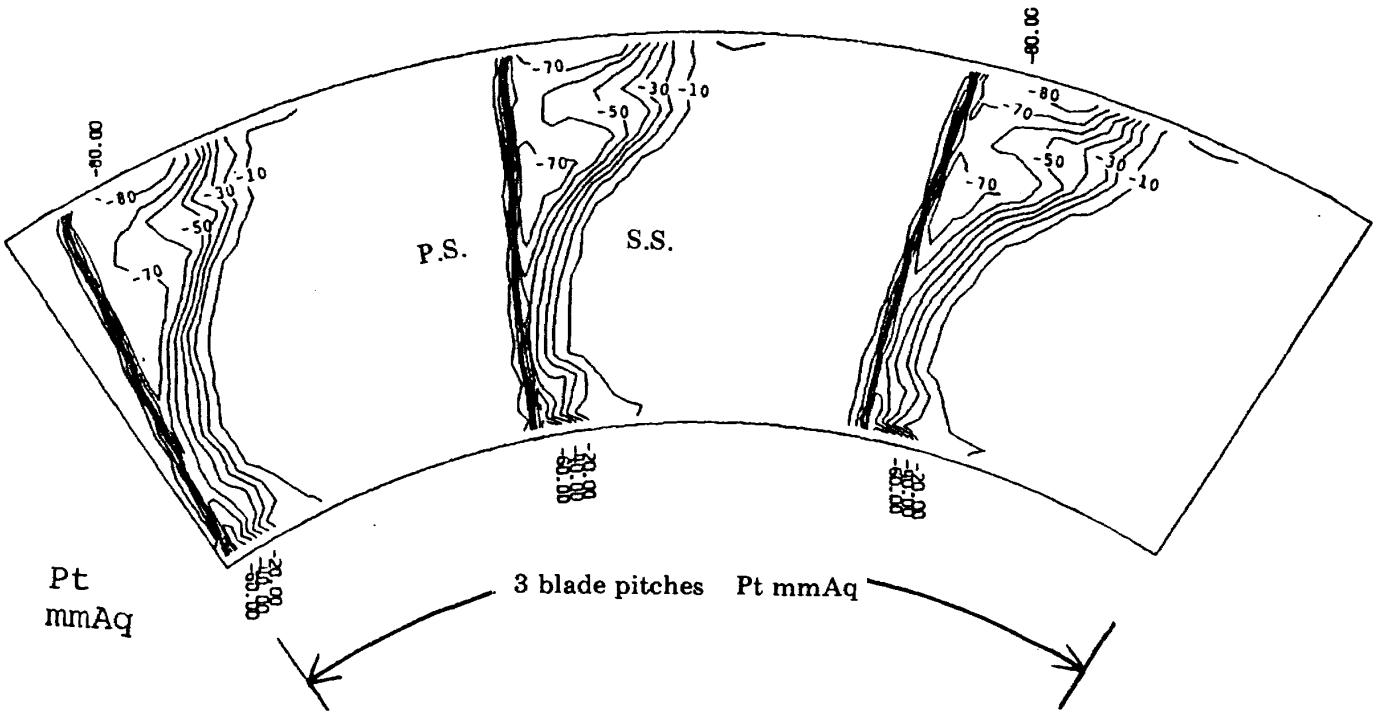

Fig. 5 Downstream flow field (Plane 4)

contain blade tip leakage flow. The outer vortex corresponds to a passage vortex which may include the horseshoe vortex comming from the leading edge of the adjacent blade. The inner one rotates in the same direction as the outer vortex and is considered a vortex separated from the trailing edge. In the present case of annular cascades in contrast to linear cascades, the vortices are pushed toward the hub due to the radial static pressure gradient (Fig. 6(b)). The inner vortex is, therefore, easily dissipated by viscous friction with the hub endwall but the outer vortex is free from the friction with the tip endwall.

The wake line here is inclined away from radial direction and is deformed by the secondary flows. The figure indicates that three peaks of total pressure deficit exist in the wake region; Ⓐ in the hub endwall region where low energy fluid migrates inward through the wake under the influence of the spanwise pressure gradient, Ⓑ in the vicinity of the outer vortex center and Ⓒ near the suction-side tip endwall where the outer vortex interacts with the strong tip-leakage flow.

The static pressure contours at 0 and 1800 rpm are shown by solid and dash lines in Fig. 6(b) which shows the pressure gradient in the radial direction and the non-uniformity in the circumferential direction at plane 5.

To illustrate variation of hub endwall boundary layer at three axially different planes, the velocity distributions of Vm are given in Fig. 7. The hub endwall boundary layer at plane 5 is uniformly developed over the hub endwall.

At Plane 6. As was shown in Fig. 7, the hub end-wall boundary layer at plane 6 is circumferentially non-uniform. This is the result that due to the more intense roll-up of the inner vortex near the hub endwall as shown in Fig. 8 (plane 6), the boundary layer is scraped from the endwall by the vortex. The outer vortex, however, continues to decay at plane 6 due to the mixing of flows. The wake inclines more and diffuses more widely at plane 6 than at plane 5, and the peak of total pressure deficit at the hub (Ⓐ in Fig. 6) is pushed to the free stream side as shown in Fig. 8(a).

At Plane 7. The wakes have become indistinct as shown in Fig. 8 (plane 7), and the inner vortex starts decaying due to viscous friction

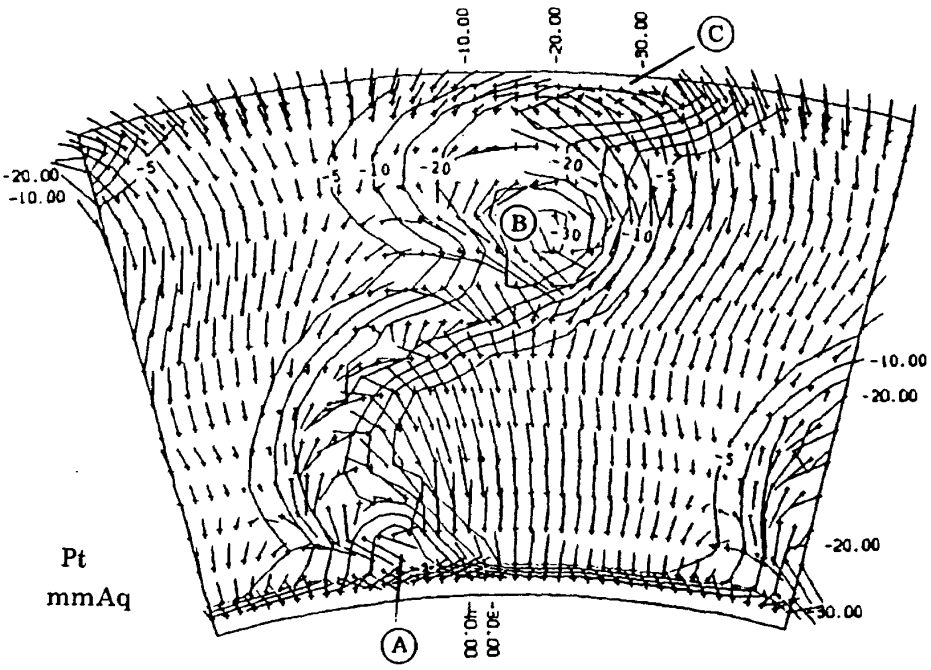

$\Delta\vec{V}s$ ⟵ 5m/sec

(a) Secondary flow vectors and total pressures

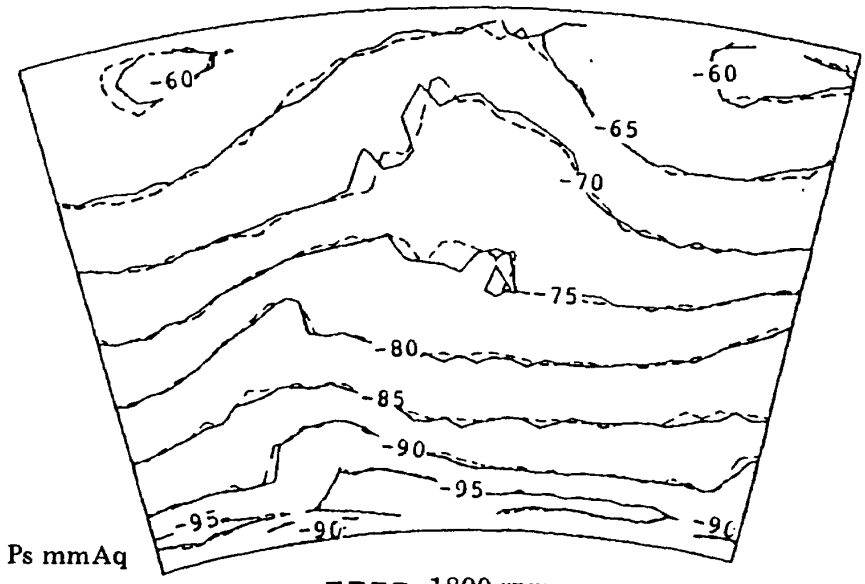

---- 1800 rpm

——— 0 rpm

(b) Static pressures

Fig. 6 Downstream flow field (Plane 5)

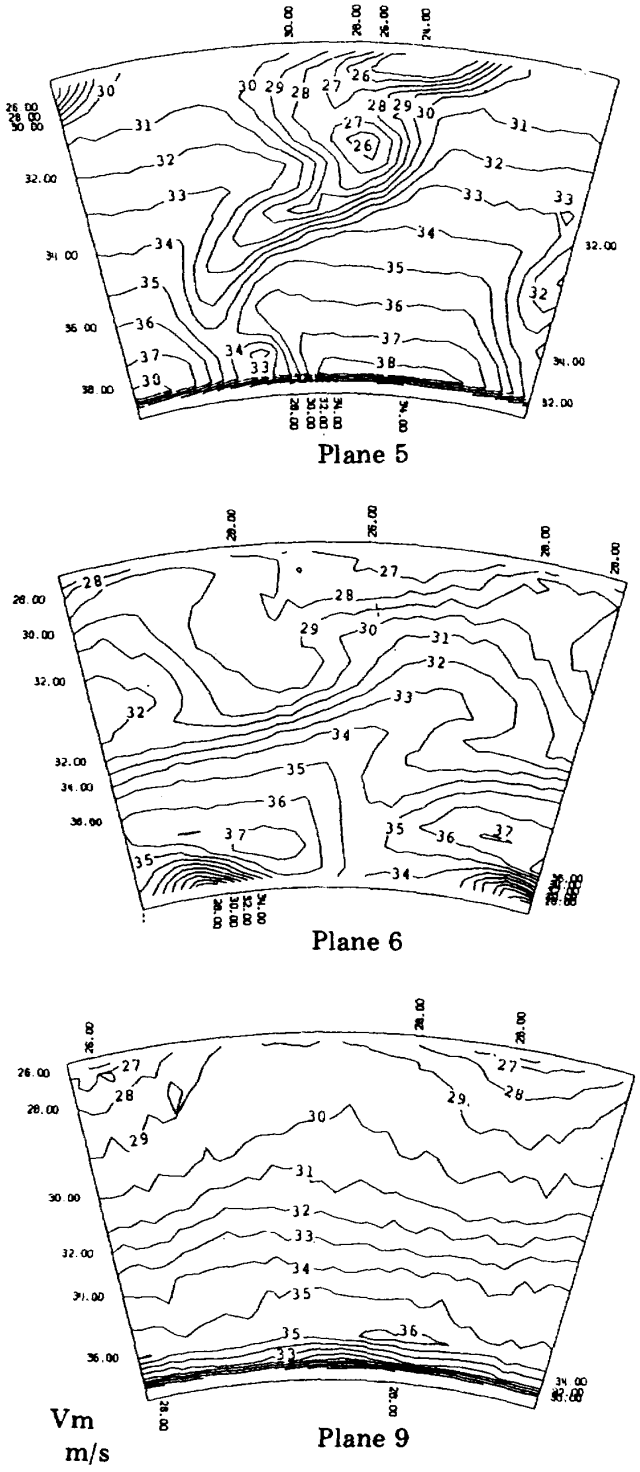

Fig. 7 Downstream flow fields, Velocity Vm (Planes 5, 6 and 9)

with the hub endwall. The outer vortex continues to decay with keeping the vortex center at almost the same radial position. On the other hand, the static pressure at this plane is almost uniform circumferentially as shown in Fig. 8(b).

At Planes 8 and 9. As seen in Fig. 8(a), the inner vortex decays very quickly and disappears almost completely at the furthest downstream plane 9 tested (about 4.26 times the blade chord downstream of the stator along the mean flow direction). The hub endwall boundary layer (Fig. 7) becomes circumferentially uniform but fairly thickend. The outer vortex can still be seen and is accompanied by a new vortex induced by the interaction between the outer vortex and the radially outward flow. The pair vortices rotating in opposite directions each other look like the Taylor-Goertler vortices observed over concave surfaces[10]. An oil flow visualization made on the transparent outer endwall between planes 8 and 9 indicated many rows of streaks, also showing the possibility of such vortices.

Effects of Downstream Hub-Endwall Rotation

Fig. 9 shows effects of the hub endwall rotation on the secondary flows and on the total pressure using ΔVs or ΔPt. Four sets of three figures corresponds to the measuring planes 6, 7, 8 and 9. At plane 5 which is located over the stationary hub endwall upstream of the rotating hub, the secondary flows and the pressure were not affected and the results were omitted. Planes 6 and 7 are located over the rotating hub, plane 8 is just downstream of the rotating hub, and plane 9 is over the downstream stationary hub endwall.

When the hub endwall rotates, the total pressure loss near the hub decreases (ΔPt>0) due to the energy transfer (from the rotating endwall to the low-energy fluids on the endwall) by the viscous friction; The hub endwall boundary layer (Fig. 10) becomes much thinner at plane 9 with the endwall rotation (compared to Fig. 7 without the rotation). This friction gives radial momentum to the fluids near the endwall (or centrifugal force against the radial static pressure gradient) and causes outward secondary flows, especially

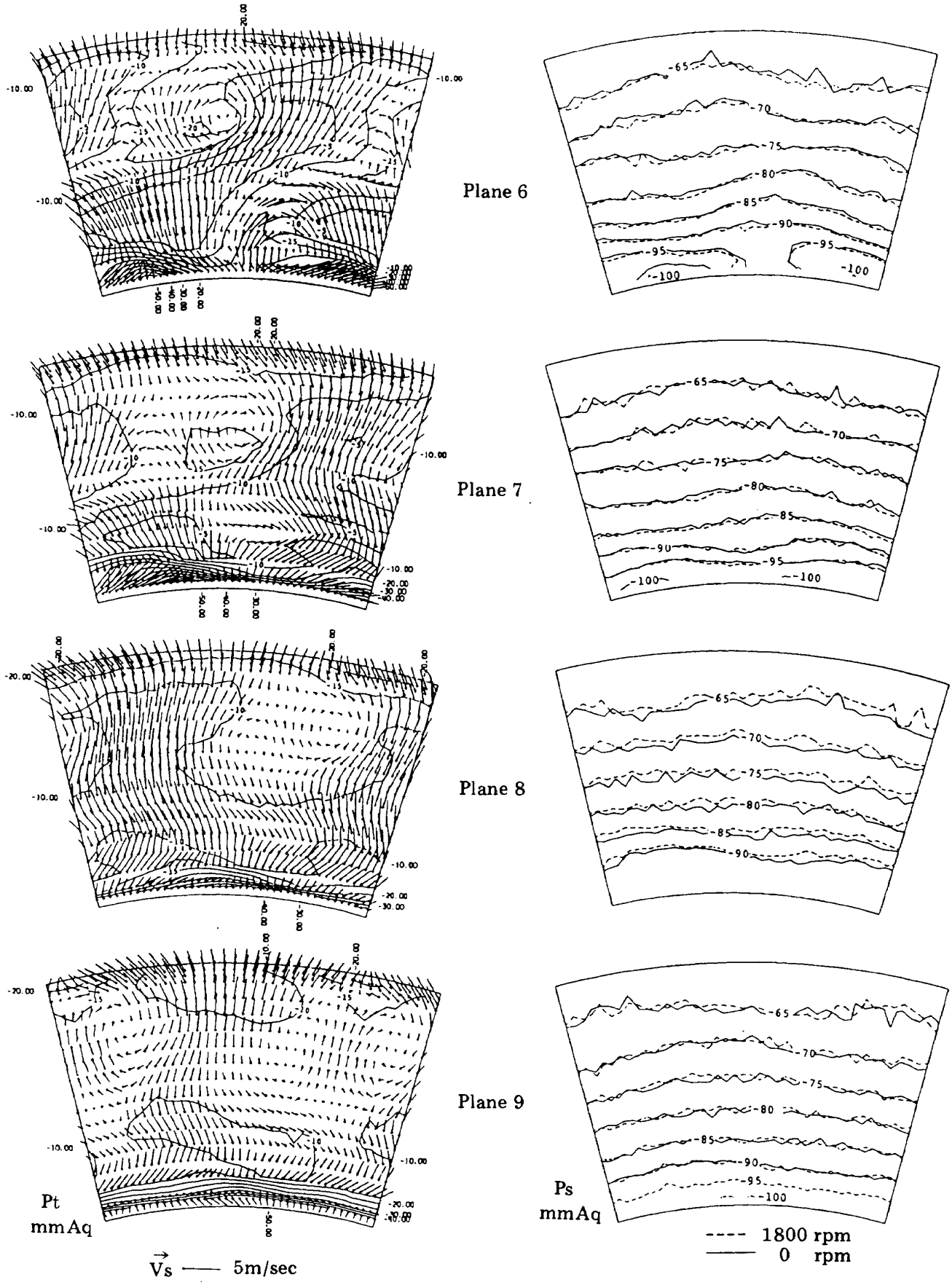

(a) Secondary flow vectors and total pressures

(b) Static pressures

Fig. 8 Downstream flow fields (Plane 6—9)

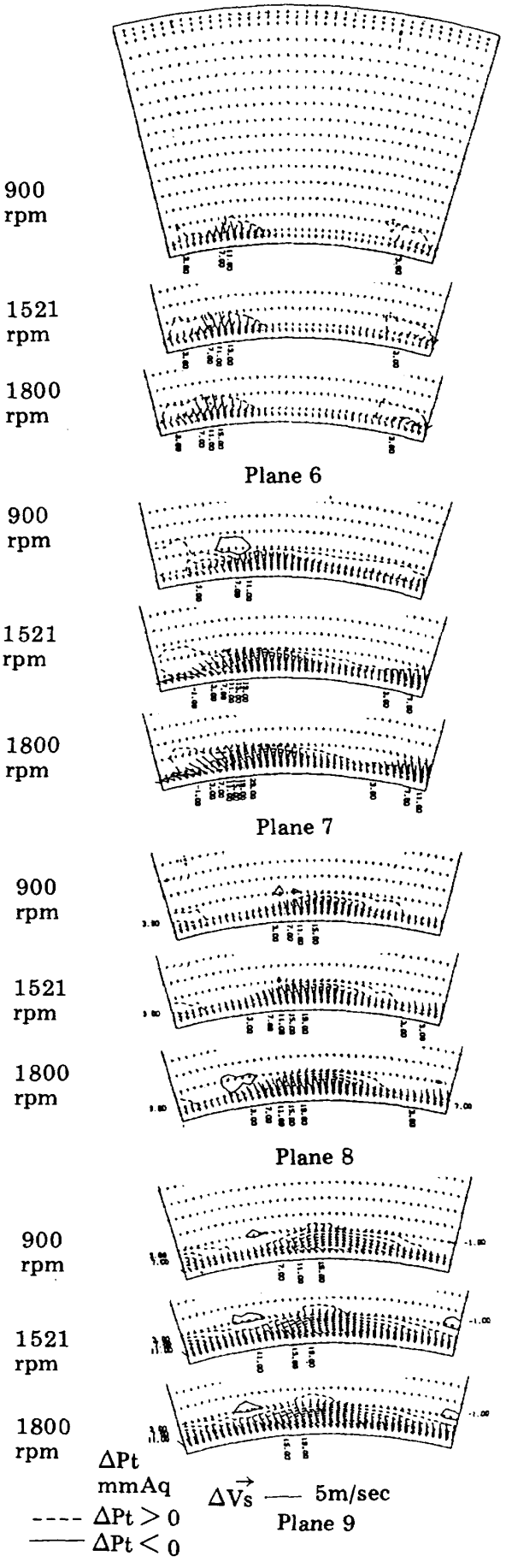

Fig. 9 Effects of rotor hub rotation

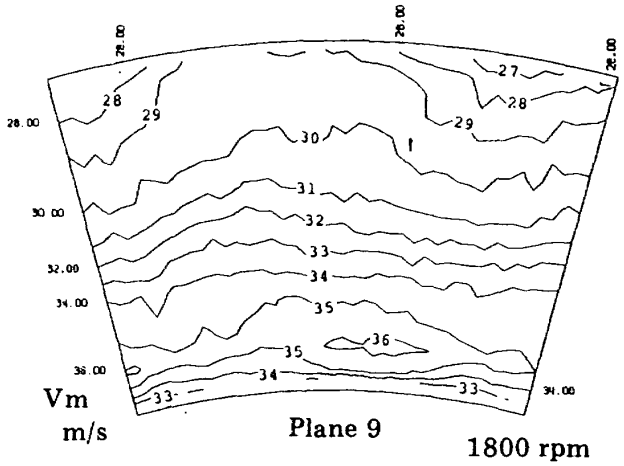

Fig. 10 Effects of rotor hub rotation, Velocity Vm

in the low-energy fluid region. The effect, however, is limited to the area near the hub endwall. The static pressure is little affected by the rotation as already given in Fig. 8(b).

Effects of Injection from Hub Endwall Slit

Figs. 11 and 12 shows the effects of air injection. The injection has a slight effect on the flow field at plane 5, although the plane is located upstream of the injection slit. The effect is strongest at plane 6 which is located just downstream of the injection slit; The loss due to fluid mixing is not circumferentially uniform and the effect is stronger in the lower-energy fluid region as was seen in the case with the rotating hub endwall. At any planes from 6 to 9 (Figs. 11 and 12), the injection generally induces inward secondary flows and increases the pressure losses. This result is contrary to that of the hub endwall rotation. The effects are not limited to the hub endwall region and can be seen even near the tip endwall. There are also some regions where the loss decreases; In these regions (surrounded by dash lines), the secondary flows are strengthened outward.

The static pressure were little influenced by the injection as shown in Fig. 13 (plane 6, for example).

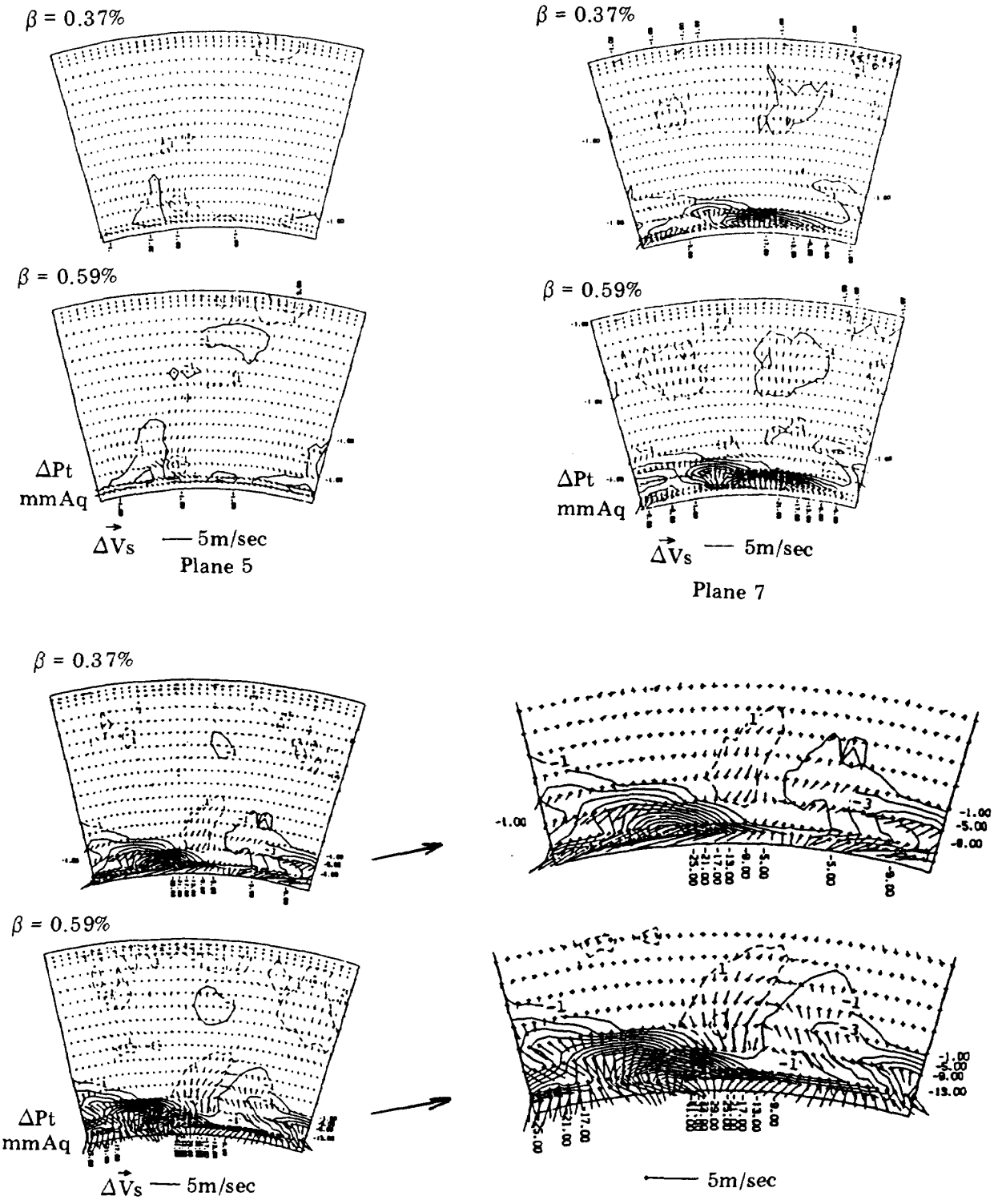

Fig. 11 Effects of injection from hub wall slit,
Differences of Vs and Pt

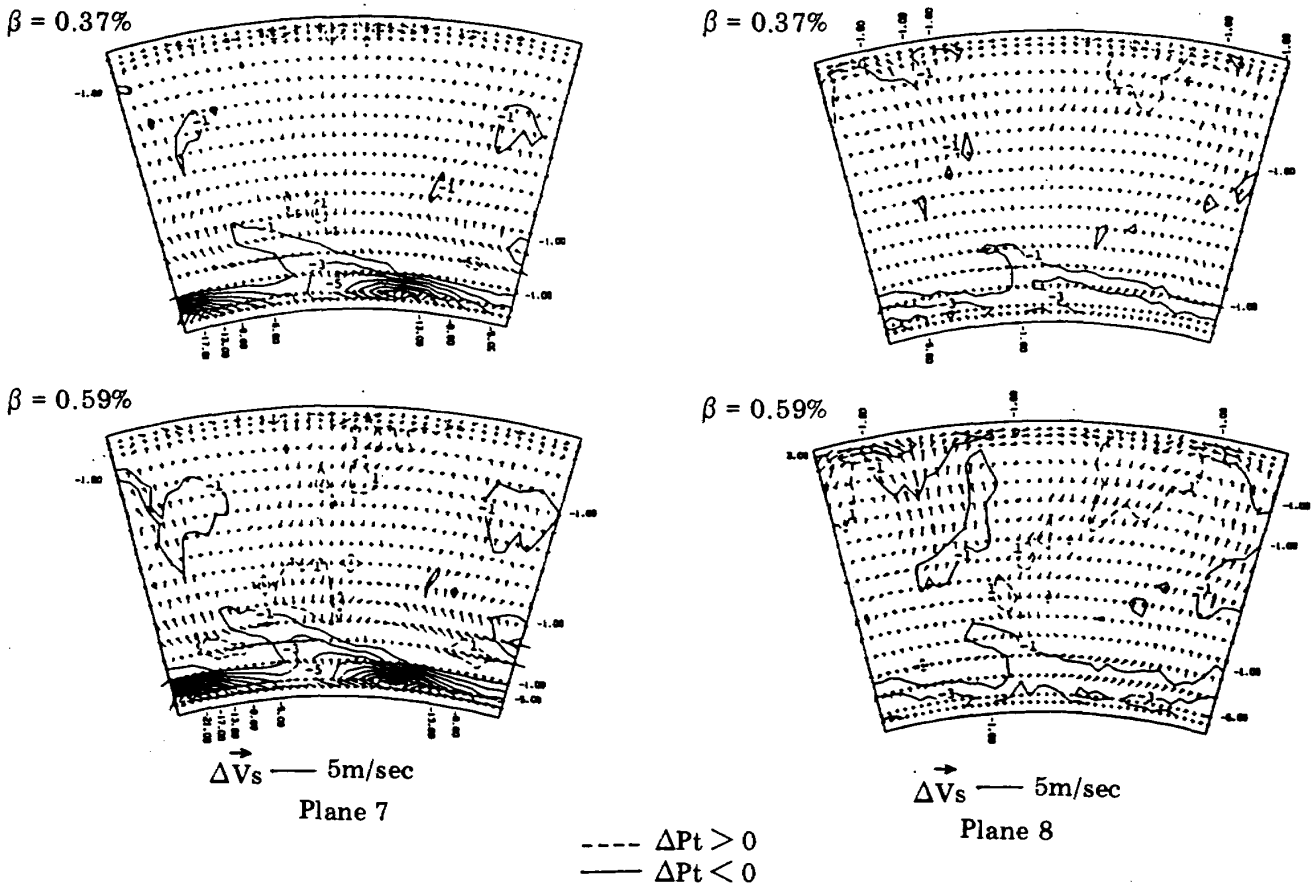

Fig. 12 Effects of injection from hub wall slit, Differences of Vs and Pt

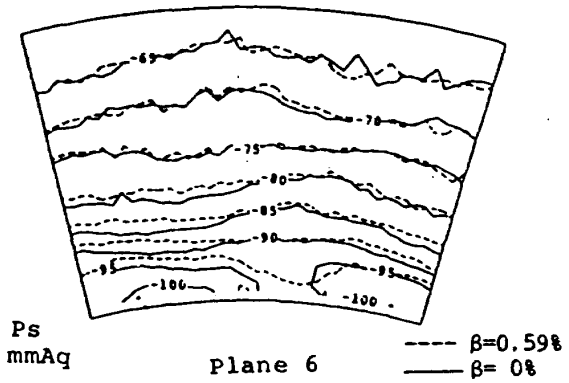

Fig. 13 Effects of injection from hub wall slit, Static pressures

Conclusions

1. Shape of the wake varies downstream of the cascade and the secondary vortices (i.e., an outer and an inner vortices seen in the present cascade) play a major role in the variation.

2. After being released from the stator cascade, the inner vortex near the hub endwall rolls up strongly once. The strong vortex scrapes the boundary layer and makes the hub endwall boundary layer thickness circumferentially non-uniform. The vortex then starts being dissipated quickly due to viscous friction with the hub endwall.

3. The outer vortex is pushed inward due to the radial pressure gradient in the annular cascade passage and gradually decays downstream of the cascade. The center of the vortex is located at almost the same radial position since the effect of friction with the outer endwall is weak.

4. It is observed that the outer vortex interacts with the radially outward (secondary) flows and forms pairs of vortices rotating in opposite directions, like the Taylor-Goertier vortices.

5. The rotation of the hub endwall supplies energy to the lower-energy fluids near the end-

wall. This induces outward secondary flows and reduces the pressure losses there. The boundary layer becomes much thinner at the downstream plane of the rotating hub.

6. A small amount of air injected from the hub endwall slit induces inward secondary flows and increases the total pressure losses due to the mixing with the main stream. The effect is again stronger in the lower-energy-fluid region near the hub endwall and the boundary layer becomes circumferentially nonuniform. The effects are not limited to the region near the hub endwall and sometimes reach the tip endwall.

Acknowledgements

The authors wish to thank Mr. T. Torisaki, formery Deputy Director-General, for his support of the present study. The financial support provided by the Ministry of International Trade and Industry as a part of the national project for a high efficiency gas turbine is gratefully acknowledged.

References

1. Sjolander, S.A., "The Endwall Boundary Layer in an Annular Cascade of Turbine Nozzle Guide Vanes", Carleton U., TR ME/A 75-4, 1975.
2. Sieverding, C.H., Van Hove, W. and Boletis, E., "Experimental Study of the Three-Dimensional Flow Field in an Annular Turbine Nozzle Guidevane", ASME Paper No. 83-GT-120, 1982.
3. Hunter, I.H., "Endwall Boundary Layer Flows and Losses in an Axial Turbine Stage", ASME Journal of Engineering for Power, Vol. 104, Jan. 1982, pp. 184—193.
4. Moustapha, S.H., Paron, G.J., and Wade, J.H.T., "Secondary Flows in Cascades of Highly Loaded Turbine Blades", ASME Journal of Engineering for Gas Turbines and Power, Vol. 107, No. 4, 1985, pp. 1031—1038.
5. Yamamoto, A. and Yanagi, R., "Production and Development of Secondary Flows and Losses Within a Three-Dimensional Turbine Stator Cascade", International Journal of Turbo and Jet-Engines, Vol. 3, No. 1, 1986, pp. 79—90 (or ASME Paper No. 85-GT-135).
6. Yamamoto, A., and Usui, H., "Study of Internal Flows in Cooled Three Dimensional Blade Rows", Part 1 and 2, Trans. JSME, Vol. 51, No. 463, 1985, pp. 829—846 (in Japanese).
7. Kind, R.J., and Yowakim, F.M., "Mean Flow and Turbulence Measurements of Annular Swirling Flows", ASME Journal of Fluid Engineering, Vol. 110, 1988, pp. 257—263.
8. Yamamoto, A. et al., "An Aerodynamic Design and the Overall Stage Performance of an Air-Cooled Axial-Flow Turbine", National Aerospace Laboratory, TR-321T, 1981 (or NASA TT F-16083, 1973).
9. Whitney, W.J. et al., "Cold-Air Investigation of a Turbine for High-Temperature-Engine Application, I. Turbine Design and Overall Stator Performance", NASA TN D-3751, 1966.
10. Schlichting, H., "Boundary-Layer Theory", Mcgraw-Hill Book Company, 1968, pp. 500—509 (on stability of a boundary layer).
11. A. Yamamoto and H. Nouse, "Transient Phenomena of Secondary Flows and Losses downstream a Three Dimensional Turbine Stator Cascade with/without the Effects of Hub Rotation and of Hub Injection", Symposium on Multi-Dimensional Fluid Transients, ASME Winter Annual Meeting, FED-Vol. 18, pp. 51—59, Dec. 1984.

TECHNICAL REPORT OF NATIONAL
AEROSPACE LABORATORY
TR-1021T

航空宇宙技術研究所報告1021T号(欧文)

平成元年4月発行

発行所　航空宇宙技術研究所
東京都調布市深大寺東町7丁目44番地1
電話 三鷹(0422)47-5911(大代表) 〒182
印刷所　株式会社 実業公報社
東京都千代田区九段南4 2-12

Published by
NATIONAL AEROSPACE LABORATORY
7-44-1 Jindaijihigashi machi, Chōfu, Tokyo
JAPAN

Printed in Japan